

A Vibration-Based Approach for Stator Winding Fault Diagnosis of Induction Motors: Application of Envelope Analysis

Chao Jin¹, Agusmian P. Ompusunggu², Zongchang Liu¹, Hossein D. Ardakani¹, Fredrik Petré², and Jay Lee¹

¹NSF I/UCRC Center for Intelligent Maintenance Systems (IMS), Cincinnati, OH, 45221, USA

jinco@mail.uc.edu
liuzc@mail.uc.edu
davarihn@mail.uc.edu
jay.lee@uc.edu

²Flanders' Mechatronics Technology Centre (FMTC), Heverlee, 3001, Belgium

agusmian.ompusunggu@fmtc.be
frederik.petre@fmtc.be

ABSTRACT

Induction motors are usually considered as one of the key components in various applications. To maintain the availability of induction motors, it calls for a reliable condition monitoring and prognostics strategy. Among the common induction motor faults, stator winding faults are usually diagnosed with current and voltage signals. However, if the same performance can be achieved, the use of vibration signal is favorable because the winding fault diagnostic method can be integrated with bearing fault diagnostic method which has been successfully proven with vibration signal. Existing work concerning vibration for winding faults often takes it either as auxiliary to magnetic flux, or is not able to detect the winding faults unless severity is already quite significant. This paper proposes a winding fault diagnostic method based on vibration signals measured on the mechanical structure of an induction motor. In order to identify the signature of faults, time synchronous averaging was firstly applied on the raw vibration signals to remove discrete frequency components originating from the dynamics of the shaft and/or gears, and the spectral kurtosis filtering was subsequently applied on the residual signal to emphasize the impulsiveness. For the purpose of enhancing the residual signal in practice, a demodulation technique was implemented with the help of kurtogram. A series of experiments have been conducted on a three-phase induction motor test bed, where stator inter-turn faults can be easily simulated at different loads, speeds and severity levels. The experimental results show that the proposed method was able to detect inter-turn faults in the induction

Chao Jin et al. This is an open-access article distributed under the terms of the Creative Commons Attribution 3.0 United States License, which permits unrestricted use, distribution, and reproduction in any medium, provided the original author and source are credited.

motor, even when the fault is incipient.

1. INTRODUCTION

Three-phase induction motors play a vital role in many engineering areas such as high-speed trains, electric vehicles, industrial robots, and machine tools, etc. Unexpected failures of induction motors occurring in these machines can thus lead to excessive downtime and large losses in terms of maintenance cost and lost revenue. Condition-based maintenance (CBM) and predictive maintenance (PdM) have been proven to be a maintenance strategy that can reduce unscheduled downtime and maintenance cost. In CBM, one does not schedule maintenance activities for machines merely according to history of maintenance records and fixed maintenance rules, but also based on the prediction of machine health conditions from sensor data, so that the waste owing to redundant maintenance and failures will be avoided. Such maintenance strategy requires the technologies of: (a) on-line condition monitoring, (b) fault detection and diagnosis, and (c) prognostics.

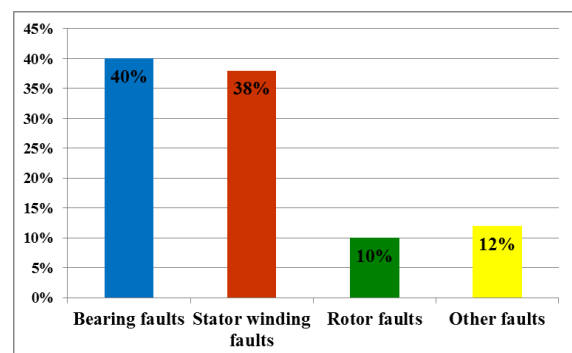


Figure 1. Statistics of failure modes in induction motors

Figure 1 shows the statistical distribution of common failure modes typically occurring in induction motors. Rolling-element bearing and stator winding failures due to insulation degradation contributes to 80% of the causes for unexpected breakdown in induction motors (Jover Rodríguez & Arkkio, 2008). Condition monitoring, diagnosis, and prognostics for rolling-element bearings have been well studied during the past four decades due to its wide applications in almost all the rotary machinery. Vibration-based and motor current signature analysis (MCSA) based monitoring methods for roller-element bearings in induction motors have been widely published in literature. However, the condition monitoring for winding insulation faults, especially vibration-based diagnosis and prognosis methods remain limited.

Winding faults due to insulation degradation can be classified into four types (Ukil, Chen and Andenna, 2011), namely (a) inter-turn short of the same phase, (b) short between coils of same phase, (c) short between two phases, and (d) short between phase to earth. Among them, inter-turn fault is considered to be the most challenging winding fault to be detected in induction motors. The online condition monitoring methods for motor winding faults are summarized in Figure 2. Most of the online monitoring methods are based on current and voltage signals, among which the symmetric component current balance monitoring (Furfari & Brittain, 2002; Eftekhari, Moallem, Sadri and Hsieh, 2013), negative sequence impedance detector (Kliman, Premerlani, Koegl and Hoeweler, 1996), voltage mismatch (Sottile, Trutt and Kohler, 2000; Trutt, Sottile and Kohler, 2002), and Parks vector (Cardoso, 1997) are the most widely referred methods. Nevertheless, these methods require measuring 3-phase high voltage signal from induction motors, which requires expensive sensors and DAQ hardware. Moreover, direct measurements of 3-phase voltages from motor windings are not feasible for online application, and the voltage measurements from the frequency-inverter drive are usually pulse-width modulation (PWM) signals that need additional signal processing process.

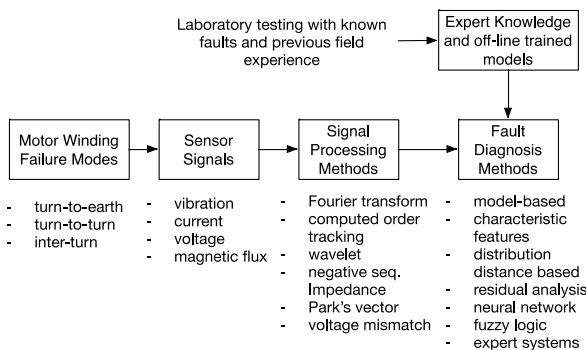


Figure 2. Online condition monitoring methods for motor winding fault (Sin, Soong and Ertugrul, 2003)

Compared with the current and voltage-based winding fault monitoring, vibration-based methods have the advantages of (a) requiring less expensive sensors, (b) requiring less channels for the DAQ system, and (c) monitoring mechanical failures at the same time. Yet vibration analysis for motor winding fault detection has received modest attention due to claimed lower sensitivity. To remedy this gap, this paper proposes a combination of different signal processing techniques to mine and amplify the motor winding fault related features. Time synchronous averaging, spectral kurtosis filtering, and envelope analysis are implemented in the signal processing process. As will be discussed in the results section, the first order of envelope spectrum showed monotonically increasing trend as the level of winding insulation degradation increase.

The remaining part of the paper will be organized as follows: Section 2 discusses the methodology development and theoretical background of the signal processing techniques applied to the motor vibration signals; Section 3 briefly discusses the experimental setup and the test procedure for data generation; Section 4 demonstrates the effectiveness of the proposed vibration signal processing methods and the selected features through the experimental data analysis; and Section 5 summarizes the important findings obtained in this study.

2. METHODOLOGY DEVELOPMENT

2.1. Overall Method

Vibration signal has long been adopted for the diagnosis of mechanical wear in rotary machinery, such as bearings and gearboxes (Randall & Antoni, 2011). One of the elementary assumptions of vibration analysis for rotary machinery mechanical faults is that the concerned fault leads to impulses in vibration signals, which do not occur in the healthy state. Detection of the impulses hidden in the smearing and noise requires advanced signal processing techniques to emphasize the impulsiveness, especially when the fault is incipient. Similar to mechanical faults, induction motor winding faults will generate additional magnetomotive force that is usually reflected in the vibration signal at harmonics of slot frequency and supply frequency (Lamim Filho, Pederiva and Brito, 2014). However, these characteristics are only significant when the faulty turns are around 5% of total windings (Lamim, Brito, Silva and Pederiva, 2013), making it difficult to detect winding faults at an early stage.

Inspired by bearing fault diagnosis, this paper addresses the issue when the inter-turn faults are still preliminary by adopting advanced signal processing tools. As shown in Figure 3, the first step of signal processing was to check the vibration data quality (Jabłoński, Barszcz and Bielecka, 2011; Jablonski & Barszcz, 2013) to guarantee raw data integrity and justify the correctness in the following

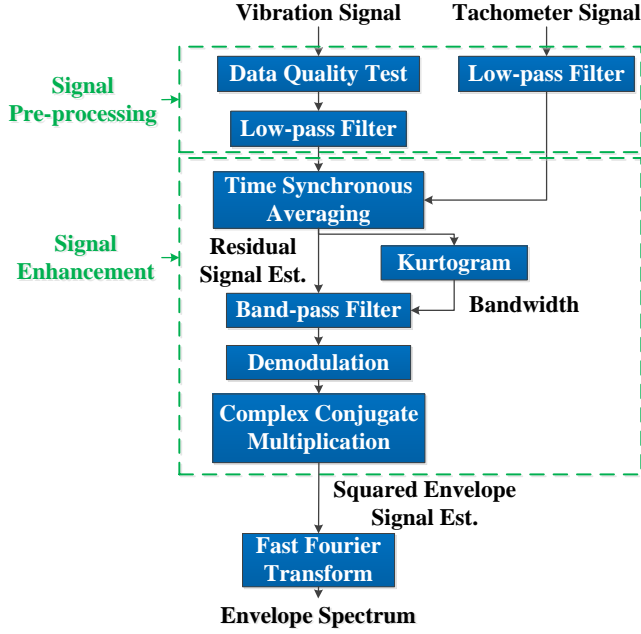


Figure 3. Flowchart of inter-turn fault detection for three-phase induction motors using vibration signal.

analysis. Then, the “corrected” vibration signal and the tachometer signal passed through a low-pass filter to exclude the high frequency noise. The cut-off frequency was set to be one fourth of sampling frequency (in this case 12800 Hz) for the vibration signal, and 10 Hz for the tachometer signal, since the ratio of tachometer is 1/4. After the aforementioned pre-processing steps, time synchronous averaging (TSA) was performed to eliminate discrete frequency component noise (Randall & Antoni, 2011). Then the resonance frequency section of the obtained residual signal estimate with TSA that contained faulty characteristics was enhanced by envelope analysis, whose bandwidth was selected using kurtogram.

The following sub-sections focus on introducing the theoretical background of the tools utilized and explaining why they are effective in detecting inter-turn faults in induction motors.

2.2. Theoretical Background

Instead of going through the calculation of magnetic forces, the induction motor winding fault detection strategy is formulated from the perspective of vibration signal processing. To state mathematically, the problem is to detect the inter-turn faulty signal $x(t)$ buried in the noise $\eta(t)$. And the actual raw signal $s(t)$ we get is the combination of the two, which is (Antoni & Randall, 2006)

$$s(t) = x(t) + \eta(t) \quad (1)$$

Under this problem statement, the following assumptions for this research are proposed:

1. The inter-turn faulty signal $x(t)$ has transients and contains impulses which do not occur or follow a different pattern in the healthy conditions;
2. The noise $\eta(t)$ refers to not only the stationary measurement noise, but also the discrete frequency component, namely the vibration influence of the mechanical parts.

2.2.1. Time synchronous averaging (TSA)

Time synchronous averaging (TSA) is an essential tool for rotating machines that extracts periodic waveforms from noisy data. TSA is performed with respect to a certain shaft according to the tachometer signal as angular position reference. Vibration signals that went through TSA process will have an integer number of orders of the fundamental harmonic (shaft frequency) retained, and other vibration components weakened. If the synchronous-averaged signal is subtracted from the original signal, the residual signal that have the harmonics of the shaft frequency removed will be obtained. Both the synchronous-averaged signal and residual signal contain diagnostic information of different failure mode (Al-Atat, Siegel and Lee, 2011). While there are many different techniques for TSA, zero crossing-based technique is the most widely used.

Zero crossing-based TSA resamples the vibration signal to angular domain where the samples recorded in one shaft rotation are interpolated into a fixed number of data points for each revolution. The number of points per revolution N is derived from Eq. (2):

$$N = 2^{\text{ceiling}(\log_2 \max(n))} \quad (2)$$

where n is the number of points between two subsequent zero crossing indices of the tachometer signal (Bechhoefer & Kingsley, 2009).

However, resampling from time domain to angular domain will cause problems for the following signal processing steps since the kernel functions of kurtogram, filtering, and envelope analysis have a constant frequency (Δt) instead of constant angle ($\Delta \theta$). Hence the synchronous-averaged signal should be interpolated back to its original time-based sampling mechanism before calculating the residual signal.

The process of obtaining residual signal from TSA is summarized as follows:

- (1) Find zero-crossing indices in the tachometer signal and calculate the zero crossing time (ZCT) with interpolation.
- (2) For each ZCT, calculate the time between ZTC_k and ZCT_{k+1} , namely, $dZCT_k$, where k is the crossing point index.

- (3) Calculate the resampled time interval: $dZCT/N$, where N is given by Eq. (2). Interpolate the signal to the newly resampled time and accumulate the resampled data.
- (4) Save the original time stamps for each revolution.
- (5) Repeat step (2) through (4) for all the revolutions, and then divide the accumulated N point vector by number of revolutions.
- (6) Interpolate the N point vector (TSA signal) back to the original time stamps for each revolution, and combine the interpolated TSA signal to get the same length of vector as the original data.
- (7) Subtract the combined vector from the original data to get the residual signal.

2.2.2. Spectral kurtosis and kurtogram

Kurtosis as a statistical feature is widely used as a global value to detect the peakiness in a signal. It is defined as

$$k = \frac{E\left[\left(x(t) - E(x(t))\right)^4\right]}{E\left[\left(x(t) - E[x(t)]\right)^2\right]^2} \quad (3)$$

where $E[\bullet]$ indicates the averaging calculation. Spectral kurtosis is an extension of kurtosis to a function of frequency, and is known for identifying the impulsiveness in the signal spectrum for rotary machinery fault diagnosis. It is calculated based on the short-time-Fourier-transform (STFT) $X(t, f)$ of the original signal. As mentioned by Randall et al in (Randall & Antoni, 2011), spectral kurtosis is defined as

$$K(f) = \frac{E\left[\left(X(t, f) - E(X(t, f))\right)^4\right]}{E\left[\left(X(t, f) - E[X(t, f)]\right)^2\right]^2} - 2 \quad (4)$$

The benefit of spectral kurtosis analysis is that it is able to find the frequency band that contains fault characteristics without requiring a large amount of history data. However, it is then of vital importance that an appropriate window length to be chosen for the STFT. In order to find the optimal window length, or equivalently bandwidth, fast kurtogram was adopted to plot spectral kurtosis against level and frequency. Another task for kurtogram is to find the center frequency with the highest spectral kurtosis value, which is related to the resonance frequency of the motor itself. The incipient vibration winding fault causes will be amplified at this resonance frequency. Reader should be able to observe in Figure 4 that the color in the fast kurtogram indicates the value of kurtosis, and in this particular example the highest kurtosis exists at Level 5.5

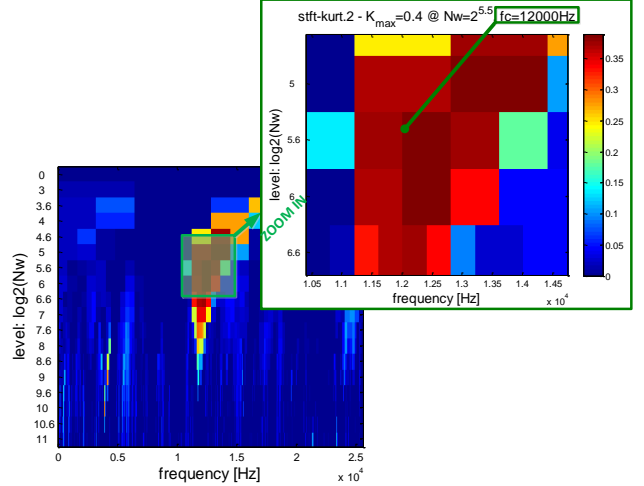


Figure 4. Kurtogram of inter-turn fault residual signal at 2000 rpm. The highest kurtosis is 0.4 at Level 5.5 with a center frequency of 12000 Hz.

with a center frequency of 12000 Hz. Even though the fast kurtogram gives the center frequency and the bandwidth, the original power spectrum density still needs to be taken into consideration to finalize the spectrum section that needs to be demodulated later. This part will be shown with graphical explanation in the following sub-section.

2.2.3. Envelope Analysis

Often, the spectrum of raw vibration signal for rotary machinery gives little insight on faulty characteristics due to noise. As mentioned in previous sections, winding faults at early stage induce mechanical impacts that are amplified at the high frequency range of the induction motor system. With kurtogram locating this high frequency range, envelope analysis will further improve the signal to noise ratio and enhance the transients so that the fault can be more easily detected.

The procedure for envelope analysis in this research is described in Figure 5, where the residual signal estimation with TSA is the input and the envelope spectrum is the output. First, a Butter band-pass filter was designed based on the center frequency and bandwidth determined from fast kurtogram. Then the resulting signal was demodulated by following Eq. (5).

$$y(t) = r(t) \times \exp(-j2\pi f_c t) \quad (5)$$

where $r(t)$ is the residual signal estimation with TSA, $j = \sqrt{-1}$, f_c is the center frequency, and $y(t)$ is the demodulated signal. Afterwards, the demodulated signal went through a low-pass filter with half of the bandwidth as the cutoff frequency. Then the squared envelope signal was calculated by following Eq. (6):

$$e(t) = y(t) \times y^*(t) \quad (6)$$

where $e(t)$ represents the squared envelope signal and $y^*(t)$ represents the complex conjugate of $y(t)$.

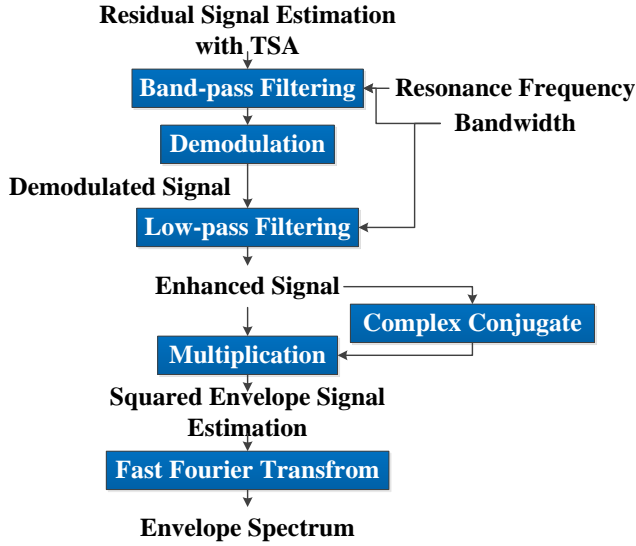


Figure 5. Flowchart of envelope analysis. The resonance frequency (center frequency) and bandwidth are determined with the help of kurtogram.

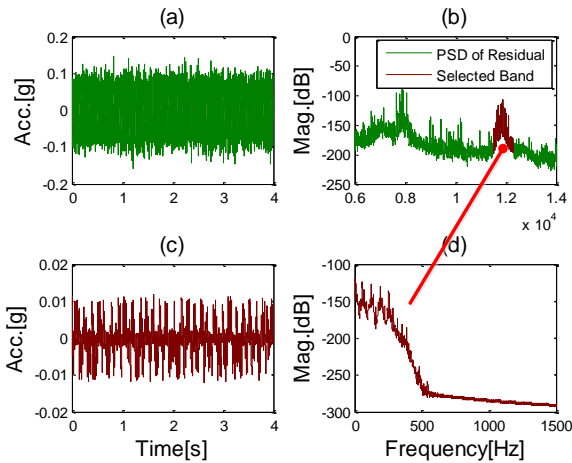


Figure 6. Comparison of time domain and frequency domain signal before and after demodulation: (a) time domain TSA residual signal estimate with kurtosis 3.0459, (b) Welch estimate power spectrum of TSA residual with high-frequency band highlighted in dark red, (c) time domain demodulated TSA residual signal with kurtosis 4.5025, (d) Welch estimate power spectrum density of the demodulated TSA residual. The signal comes from the condition of inter-turn fault. Note that the scales of plots are different.

The result of band-pass filtering and demodulation can be found in Figure 6. In time domain, the emphasis of impulsiveness in the faulty signal is recognized even graphically. Quantitatively, the kurtosis of the signal has increased from 3.1053 to 4.1744. In frequency domain, one

can clearly see in Figure 6 (b) that the peaky section centered at approx. 12000 Hz with a bandwidth of 800 Hz is highlighted. This is where the high frequency band that contains the faulty information locates. It was picked up by kurtogram and moved to lower frequency band after demodulation. Discussion on the result of envelope signal and envelope spectrum will be found in Section 4.

3. EXPERIMENTAL SETUP

For conducting this research, a dedicated induction motor test-bed was designed and developed. The test-bed is designed such that one is able to simulate the winding faults with different levels of severity and collect vibration, current, voltage and torque signals from the motor. The winding faults that could be induced in the system include (i) inter-turn and (ii) turn-to-earth faults. The test-bed was also designed to run at different speed regimes and load conditions for multi-regime data collection and analysis. The following sections will briefly describe the test-bed design, the procedure for inducing winding faults and the experiments with different fault conditions.

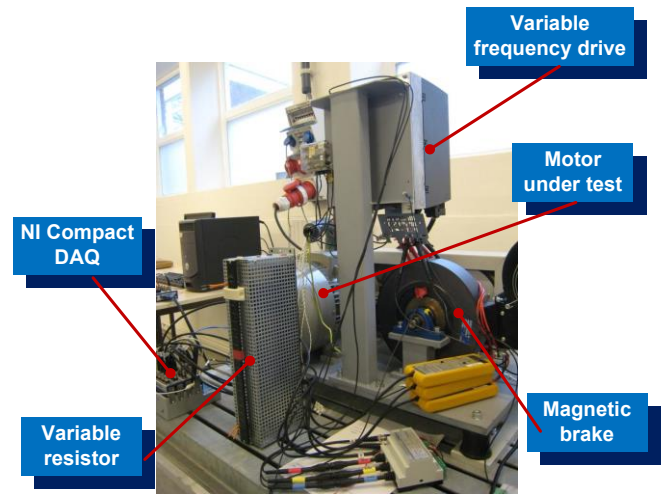


Figure 7. Photograph of the induction motor test bed.

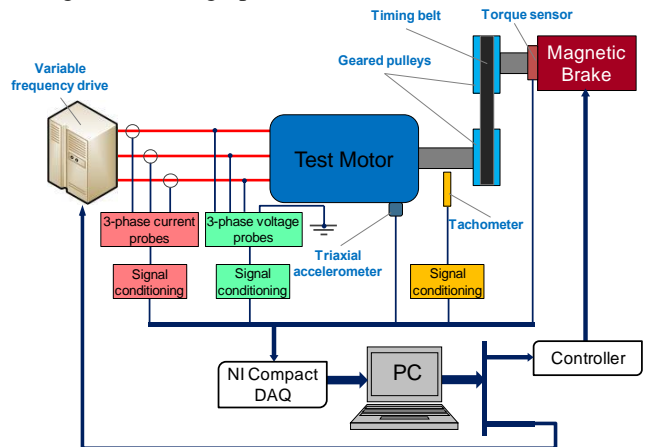


Figure 8. Schematic view of the motor test bed.

3.1. Test Setup

The test-bed consisted of an 11KW, 19.7A, 400V 3-phase induction motor driven by a variable frequency drive (VFD). The rotational speed of the motor could be varied from 0 to 3000 RPM with both stationary and transient modes available. A magnetic brake was connected to the output shaft of the motor through a timing-belt and pulley mechanism. The mechanism allowed the brake shaft to rotate at half of the speed of the motor shaft. By controlling the input current of the brake, an external load varying from 0 to 50 Nm could be applied to the motor. A PC with LabVIEW programs was used to send the control signals to the VFD and magnetic brake controller. A variable resistor with the range of 0-580 Ω was used to simulate different levels of severities in the shorted turns in inter-turn faults. A tri-axial accelerometer was mounted on the top of the housing of the motor to collect the vibration of the motor. A tachometer based on a proximity probe was used to measure the rotational speed of the motor. The head of the tachometer was put towards a 4-tooth flywheel connected to the motor shaft generating 4 pulses per revolution. The experimental setup and the schematic view of the test-bed are shown in Figure 7 and Figure 8.

3.2. Fault Simulation

The winding of the motor used in the test-bed is random-wound (Figure 9). The winding was modified by connecting three shielded wires to the coil of phase *w* at three locations and the other ends of the wires were brought outside as schematically shown in Figure 10. The inter-turn faults were simulated by connecting the other ends of the wires to a variable resistor. For healthy state simulation, the ends of the three wires were left unconnected. The inter-turn faults were simulated under two different scenarios referred to as inter-turn I and II. In inter-turn I, wires 1 (in orange) and 2 (in green) were connected through a variable resistor. Similarly for inter-turn II, wire 1 was shorted to wire 3 (black) through a variable resistor. By adjusting the resistance to 580 and 300 Ω , two levels of severity for both inter-turn I and II were simulated, as summarized in Table 1.

Table 1. Different fault levels for induction motor

State	Resistance [Ω]	Comment
F1	580	Lowest level
F2	300	Moderate level

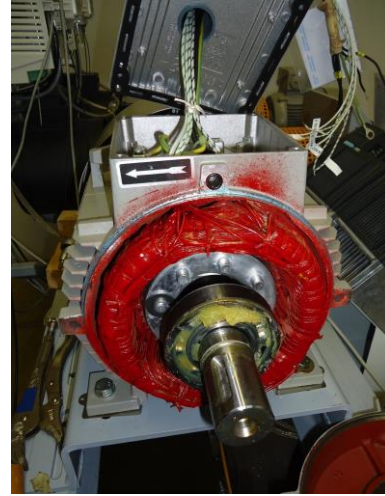


Figure 9. Disassembled motor exposing random wound stator winding.

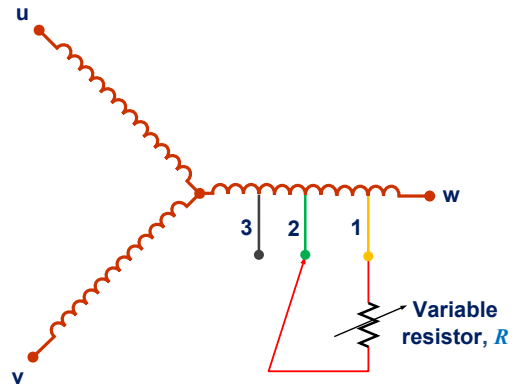


Figure 10. Schematic winding diagram with three taps on the *phase w* winding for different inter-turn fault scenarios.

3.3. Test Procedure

The test was performed at the constant speed of 2000 RPM and constant brake torque of 12 Nm for all the winding conditions. At each level of winding faults, the current i_t flowing through the variable resistor was measured and the corresponding dissipated power P_d was calculated as summarized in Table 2.

Prior to digitizing the signals, each measured signal was passed through a low-pass and an anti-aliasing filter embedded in each channel of the NI data acquisition system. Doing the tests in this way ensures that the potential aliasing problems caused by high frequency noise can be avoided. Depending on the sampling frequency, the cut-off frequency of the anti-aliasing filter was automatically adjusted. The vibration signals were sampled at the rate of 51.2 KHz with the duration of four seconds. The digitized data was stored in the PC and analyzed off-line in MATLAB software.

Table 2. Current and dissipated power through the variable resistor at different states

State	Inter-turn I		Inter-turn II	
	i_l [mA]	P_d [W]	i_l [mA]	P_d [W]
F1	265	40.7	86	4.3
F2	297	26.5	155	7.2

4. RESULTS AND DISCUSSION

Under varying fault severity levels, squared envelope signal estimation was calculated by following the procedure introduced in Section 2.2.3. The result for healthy state, Inter-turn I and Inter-turn II is presented in Figure 11. Compared with the healthy state, it is obvious that the pattern of vibration of the induction motor has changed in time domain for inter-turn fault. The period of one cycle of vibration for the healthy case is approximately 0.0456 s, and the period for both of the inter-turn cases is approximately 0.0300 s, namely 33.3 Hz which is about the same with the rotational speed (2000 RPM/60 s = 33.3 Hz). This is because inter-turn fault has changed the magnetic flux distribution of the induction motor and the faulty characteristic is related to rotating speed. It is also noticeable that the amplitude of the faulty characteristic increases as the fault becomes more severe.

After obtaining the envelope signal, Fourier transform was applied. For the purpose of comparing between different scenarios, amplitudes of the spectrum were normalized according to DC amplitude, which should be the highest; and the frequency domain was also transferred to order domain to help the readers to recognize quickly the feature at the rotational speed. In Figure 12, it is evident that at the first order, inter-turn fault case has a component. And by comparing (3) with (2) in Figure 12, the severity of the fault is also revealed.

Furthermore, a bar plot was generated for all the conditions at different severity levels, which is shown in Figure 13. As one can observe, there is a clear difference between healthy state and inter-turn faults in terms of bar height. In terms of severity, for Inter-turn I and Inter-turn II respectively, amplitudes at F2 in (b) is bigger than those in (a) of Figure 13. Besides, Inter-turn II has a larger value than Inter-turn I, which once again reveals the severity of fault successfully.

Since the values of the order domain amplitudes were normalized between 0 and 1, it can be considered as a metric called hazard value (HV) to quantify inter-turn fault in induction motors. The result is shown in Table 3.

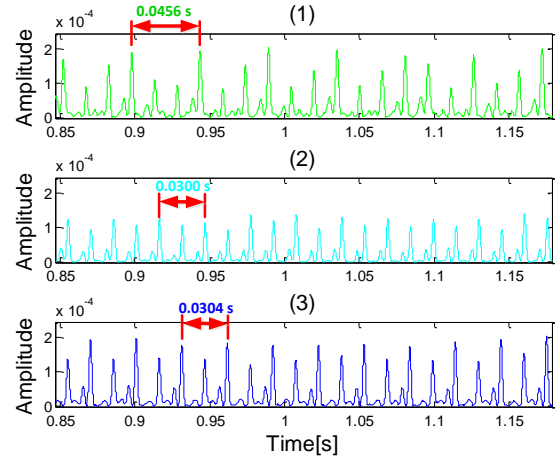


Figure 11. Time domain envelope signals for F1: (1) time domain envelope signal for healthy state with period of approx. 0.0456 s, (2) time domain envelope signal for Inter-Turn I with period of approx. 0.0300 s, (3) time domain envelope signal for Inter-Turn II with period of approx. 0.0304 s. Note that the scales of the three sub-plots are different.

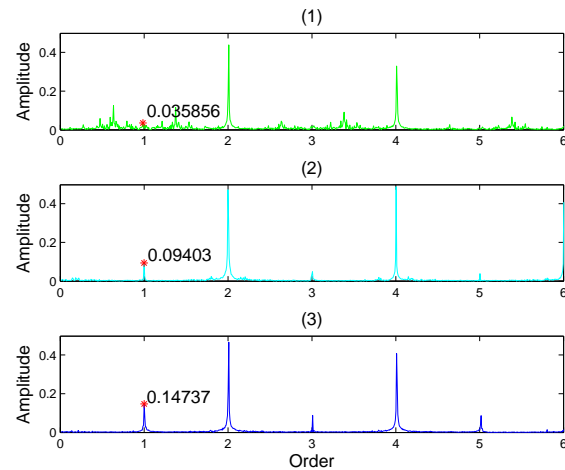


Figure 12. Envelope spectra in order domain for F1: (1) envelope spectrum for healthy state with no harmonic at the first order, (2) envelope spectrum for Inter-turn I with a peak valued at 0.09403 at the first order, (3) envelope spectrum for Inter-turn II with a peak valued at 0.14737 at the first order.

Table 3. Hazard value (HV) of different conditions and severities

Metric	Healthy	Inter-turn I		Inter-turn II	
		F1	F2	F1	F2
HV	0.0359	0.0940	0.2385	0.1474	0.2574

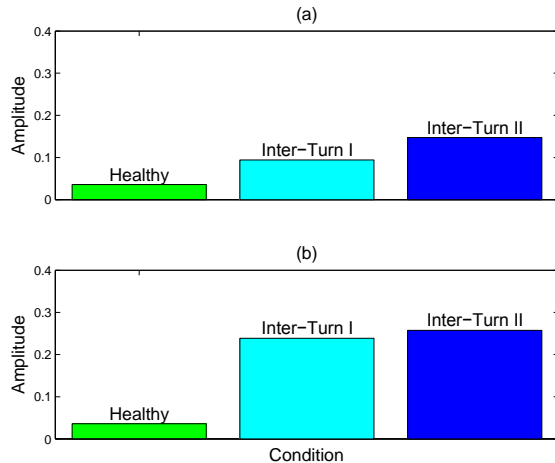


Figure 13. Amplitudes of first order component in envelope spectrum for different conditions and severity levels: (a) amplitudes for all three conditions at severity level F1, (b) amplitudes for all three conditions at severity level F2. The three colors represent healthy state, Inter-turn I, and Inter-turn II, respectively, and they are consistent with previous figures.

5. CONCLUSION

This paper proposes a vibration-based method to detect inter-turn winding fault, which is known to be the hardest to detect even with current and voltage signal. The method was divided into two stages, namely signal pre-processing stage and signal enhancement stage. In the pre-processing stage, data quality check and a low-pass filter were applied on both vibration signal and tachometer signal. In the signal enhancement stage, several techniques were adopted. Time synchronous averaging was used to remove the discrete frequency component noise, and then the residual signal was demodulated at the center frequency and bandwidth selected with the help of kurtogram. The resulting normalized envelope spectrum was converted into order domain, and the component at the first order was able to detect inter-turn fault from the healthy state, and reflect the severity. Note that this method is applied at a constant speed, and time synchronous averaging technique is in fact quite computationally costly. Other techniques to remove the discrete frequency components like cepstrum analysis are to be explored for future work.

REFERENCES

- Al-Atat, H., Siegel, D. & Lee, J. (2011). A systematic methodology for gearbox health assessment and fault classification. *Int J Prognostics Health Manage Soc*, vol. 2(1), pp. 16.
- Antoni, J. & Randall, R. (2006). The spectral kurtosis: application to the vibratory surveillance and diagnostics of rotating machines. *Mechanical Systems and Signal Processing*, vol. 20(2), pp. 308-331.
- Bechhoefer, E. & Kingsley, M. (2009). A review of time synchronous average algorithms. *Annual conference of the prognostics and health management society*
- Cardoso, A. (1997). The Park's Vector Approach: a general tool for diagnostics of electrical machines, power electronics and adjustable speed drives. *Record of the 1997 IEEE International Symposium on Diagnostics for Electrical Machines, Power Electronics and Drives, Carry-le-Rouet, France* (261-269)
- Eftekhari, M., Moallem, M., Sadri, S. & Hsieh, M.-F. (2013). Online Detection of Induction Motor's Stator Winding Short-Circuit Faults.
- Furfari, F. & Brittain, J. (2002). Charles LeGeyt Fortescue and the method of symmetrical components. *Industry Applications Magazine, IEEE*, vol. 8(3), pp. 7-9.
- Jablonski, A. & Barszcz, T. (2013). Validation of vibration measurements for heavy duty machinery diagnostics. *Mechanical Systems and Signal Processing*, vol. 38(1), pp. 248-263.
- Jabłoński, A., Barszcz, T. & Bielecka, M. (2011). Automatic validation of vibration signals in wind farm distributed monitoring systems. *Measurement*, vol. 44(10), pp. 1954-1967.
- Jover Rodríguez, P. V. & Arkkio, A. (2008). Detection of stator winding fault in induction motor using fuzzy logic. *Applied Soft Computing*, vol. 8(2), pp. 1112-1120.
- Kliman, G., Premerlani, W., Koegl, R. & Hoeweler, D. (1996). A new approach to on-line turn fault detection in AC motors. *Industry Applications Conference, 1996. Thirty-First IAS Annual Meeting, IAS'96., Conference Record of the 1996 IEEE* (687-693)
- Lamim Filho, P., Pederiva, R. & Brito, J. (2014). Detection of stator winding faults in induction machines using flux and vibration analysis. *Mechanical Systems and Signal Processing*, vol. 42(1), pp. 377-387.
- Lamim, P., Brito, J. N., Silva, V. A. D. & Pederiva, R. (2013). Detection of Electrical Faults in Induction Motors Using Vibration Analysis. *Journal of Quality in Maintenance Engineering*, vol. 19(4), pp. 2-2.
- Randall, R. B. & Antoni, J. (2011). Rolling element bearing diagnostics—a tutorial. *Mechanical Systems and Signal Processing*, vol. 25(2), pp. 485-520.
- Sin, M. L., Soong, W. L. & Ertugrul, N. (2003). Induction machine on-line condition monitoring and fault diagnosis - a survey. *Australasian Universities Power Engineering Conference* (1-6), Christchurch, New Zealand

- Sottile, J., Trutt, F. C. & Kohler, J. L. (2000). Experimental investigation of on-line methods for incipient fault detection [in induction motors]. *Industry Applications Conference* (2682-2687)
- Trutt, F. C., Sottile, J. & Kohler, J. L. (2002). Online condition monitoring of induction motors. *Industry Applications, IEEE Transactions on*, vol. 38(6), pp. 1627-1632.
- Ukil, A., Chen, S. & Andenna, A. (2011). Detection of stator short circuit faults in three-phase induction motors using motor current zero crossing instants. *Electric Power Systems Research*, vol. 81(4), pp. 1036-1044.